Heavier Inner-Core Rainfall of Major Hurricanes in the North Atlantic Basin Than in Other Global Basins

OSCAR GUZMAN[a] AND HAIYAN JIANG[a]

[a] *Department of Earth and Environment, Florida International University, Miami, Florida*

(Manuscript received 21 August 2020, in final form 1 March 2021)

ABSTRACT: Based on 19 years of precipitation data collected by the Tropical Rainfall Measuring Mission (TRMM) and the Global Precipitation Measurement (GPM) mission, a comparison of the rainfall produced by tropical cyclones (TCs) in different global basins is presented. A total of 1789 TCs were examined in the period from 1998 to 2016 by taking advantage of more than 47 737 observations of TRMM and GPM 3B42 multisatellite-derived rainfall amounts. The axisymmetric component of the TC rainfall is analyzed in all TC-prone basins. The resulting radial profiles show that major hurricanes in the Atlantic basin exhibit significantly heavier inner-core rainfall rates than those in any other basins. To explain the possible causes of this difference, rainfall distributions for major hurricanes are stratified according to different TC intensity and environmental variables. Based on the examination of these parameters, we found that the stronger rainfall rates in the Atlantic major hurricanes are associated with higher values of convective available potential energy, drier relative humidity in the low to middle troposphere, colder air temperature at 250 hPa, and stronger vertical wind shear than other basins. These results have important implications in the refining of our understanding of the mechanisms of TC rainfall.

KEYWORDS: Hurricanes/typhoons; Rainfall; Microwave observations; Remote sensing; Trends

1. Introduction

The rainfall associated with tropical cyclones (TCs) is one of the most severe events affecting infrastructure and human activities in tropical and subtropical regions. The severity of damage caused by TC rainfall has been highlighted in many recent studies (e.g., Willoughby 2012; Rappaport 2014; Park et al. 2016), which has led to more attention to this topic in the priorities of the research and forecast communities. Nowadays, significant progress in the prediction of TC rainfall has been achieved through the use of extrapolation approaches from previous satellite observations (Kidder et al. 2005; Ferraro et al. 2005), climatology and persistent methods (Lonfat et al. 2007), and modern numerical models (Biswas et al. 2017). However, compared to the outstanding advancements in the prediction of TC tracks, the quantitative precipitation forecast of TCs still shows modest skill (Lonfat et al. 2004; Tuleya et al. 2007).

In the case of the forecast techniques that use the persistence and climatological information as a starting point to predict rainfall rates, a permanent refinement of climatological features of TC rainfall is a critical step in producing more accurate results, especially for the most active areas within the TC structure like the inner-core region. One key element in this forecasting approach is the mean radial distribution of rainfall, as Lonfat et al. (2004) described. In that study, based on 3 years of rainfall estimates produced by the Tropical Rainfall Measuring Mission (TRMM) Microwave Imager (TMI), the authors examined the radial distribution of azimuthally averaged rainfall rates from the storm center to a 500-km radius. Their results suggested a close relationship between TC intensity and the precipitation rate, showing a peak in the inner-core region that ranges from 3 mm h^{-1} for tropical storms to about 12 mm h^{-1} for major hurricanes. These axisymmetric profiles have served as the foundation to construct instantaneous footprints of TC rainfall as a function of the storm intensity in forecasting models like R-CLIPER and its successor, the Parametric Hurricane Rainfall Model (PHRaM; Lonfat et al. 2007). However, adding the effect of environmental conditions in the TC rainfall forecast is still under development.

Numerous studies have also shown that the distribution of TC rainfall is affected by environmental conditions, including but not limited to factors such as humidity, wind shear, and sea surface temperature. In terms of humidity, Jiang et al. (2008a), using TRMM 3B42 observational data, found empirical relationships that explain the total volumetric rain as a function of total precipitable water, horizontal moisture convergence, and ocean surface flux for the Atlantic basin with higher correlations coefficients than previous works based on TC intensity only. In the case of wind shear, Cecil (2007), using the Special Sensor Microwave Imager (SSM/I) and TMI data, found that when TCs interact with environmental wind shear they acquire an asymmetric structure depicted by rainfall enhancement in downshear directions and to the left of the shear vector. The magnitude of this shear-related enhancement oscillates by a factor of 2 to 4 when comparing the inner 100 km with the unfavored quadrants, depending on the wind shear magnitude and distance from the TC center. Finally, in the case of the sea surface temperature (SST), Lin et al. (2015) examined the relation between TC rainfall area and the relative sea surface temperature, the latter is defined as the SST in the TC environment minus the average tropical SST (30°N–30°S). They found strong dependencies of TC rainfall area on the relative SST in all the TC intensity categories. Their study reported a weak relationship between TC size and intensity and showed that the rainfall rate increases with increasing the absolute SST, especially toward the TC center.

Corresponding author: Dr. Haiyan Jiang, haiyan.jiang@fiu.edu

DOI: 10.1175/JCLI-D-20-0668.1

TABLE 1. Number of TCs, major hurricanes, and corresponding 3B42 observations during 1998–2016 in different basins.

Variable	ATL	ECPA	NWP + NIO	SH	Total
No. of TCs	315	363	637	474	1789
3B42 observations	8567	9176	16 581	13 413	47 737
No. of major hurricanes	63	75	188	137	463
3B42 observations for major hurricanes	581	527	1798	1090	3996
No. of CAT5 hurricanes	10	8	56	23	97
3B42 observations for CAT5 hurricanes	45	22	216	76	359

Previous climatological studies provided valuable insight into better understanding the quantitative prediction of TC rainfall and their global variation. Jiang and Zipser (2010), using 8 years of TRMM data, described the contribution of TCs to total rainfall in each of the TC-prone global basins. Their study reported interbasin differences that result in an overall differential contribution of 8%–9%, 7%, 11%, 5%, 7%–8%, and 3%–4% for the North Atlantic, northeastern Pacific, northwestern Pacific, north Indian Ocean, southern Indian Ocean, and southern Pacific basins, respectively. Lonfat et al. (2004) examined the azimuthal mean rain rate in TCs in terms of different TC intensity categories and different TC-prone basins. However, they only used three years of TRMM data, and no significant tests were performed in their study, probably due to the small sample size. Therefore, the present study is motivated to refine the global TC rainfall climatology by using a much longer time series that consists of 19 years of multisatellite-derived rainfall amounts collected from the NASA TRMM and its successor the Global Precipitation Mission (GPM). Here, we mainly focus on characterizing the radial distribution of the

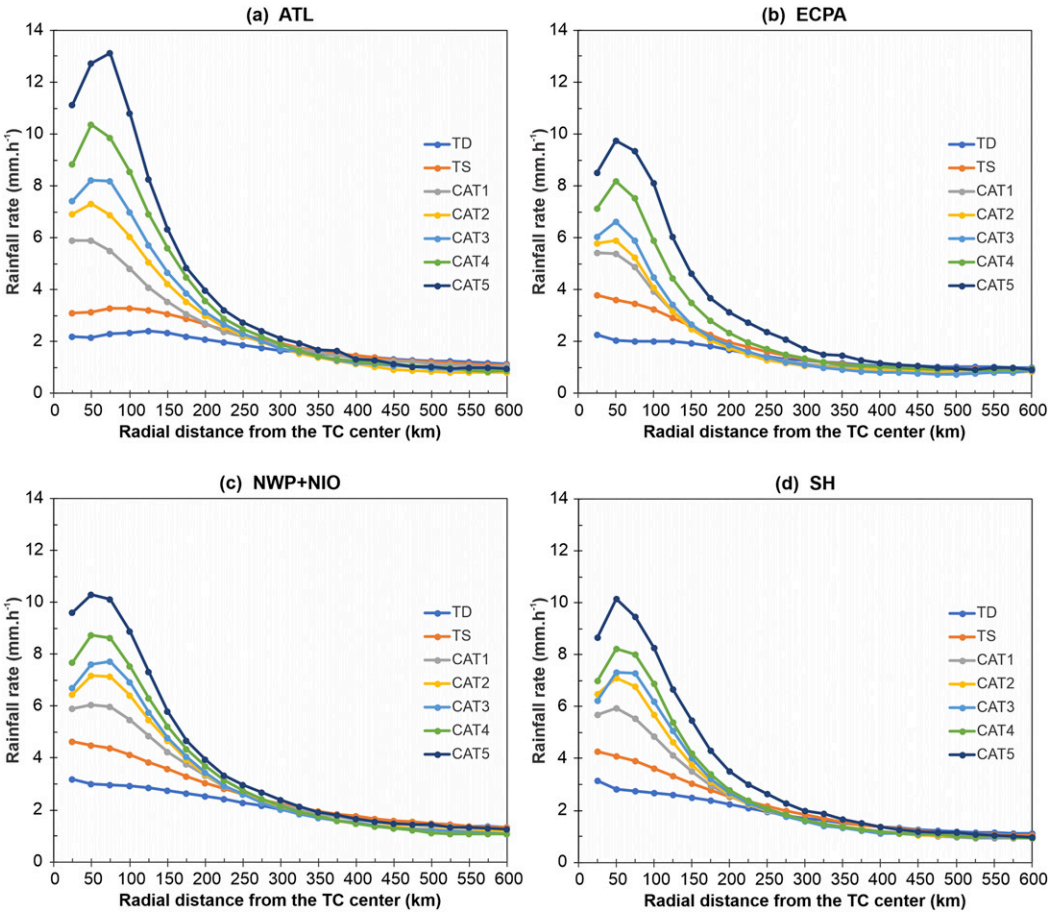

FIG. 1. Radial distribution of azimuthally averaged rainfall rate of TCs during 1998–2016 in different intensity categories in the (a) ATL, (b) ECPA, (c) NWP + NIO, and (d) SH basins.

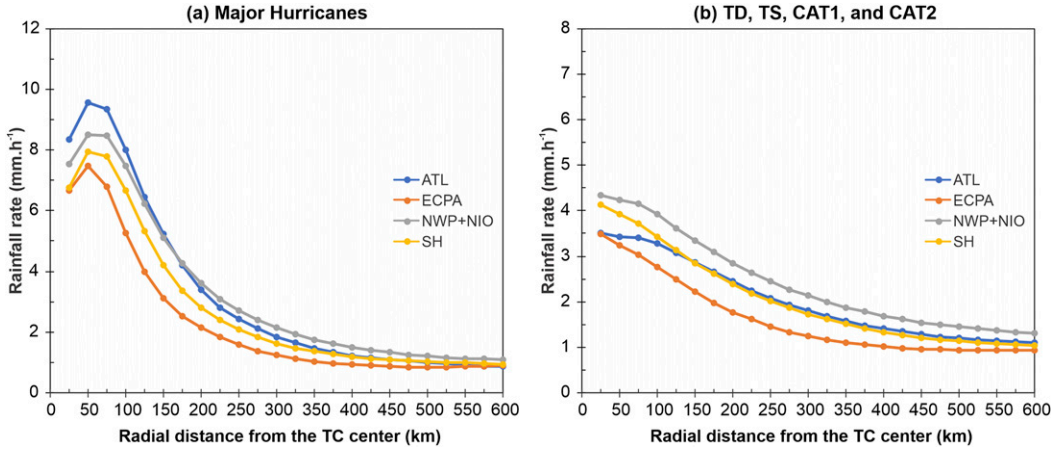

FIG. 2. Radial distribution of azimuthally averaged rainfall rate of (a) major hurricanes and (b) TCs with intensity less than major hurricanes during 1998–2016 in different basins.

azimuthal mean rainfall rates within the different global basins and different TC intensity categories. The resulting climatological differences are then linked to various potential environmental factors whose effects are examined individually to provide interbasin comparisons focused on the inner-core region of major hurricanes.

2. Data and methodology

a. Data

The analysis period spans from 1998 to 2016, covering all the TC-prone global basins grouped into four geographic zones: the northern Atlantic (ATL), the east-central Pacific (ECPA),

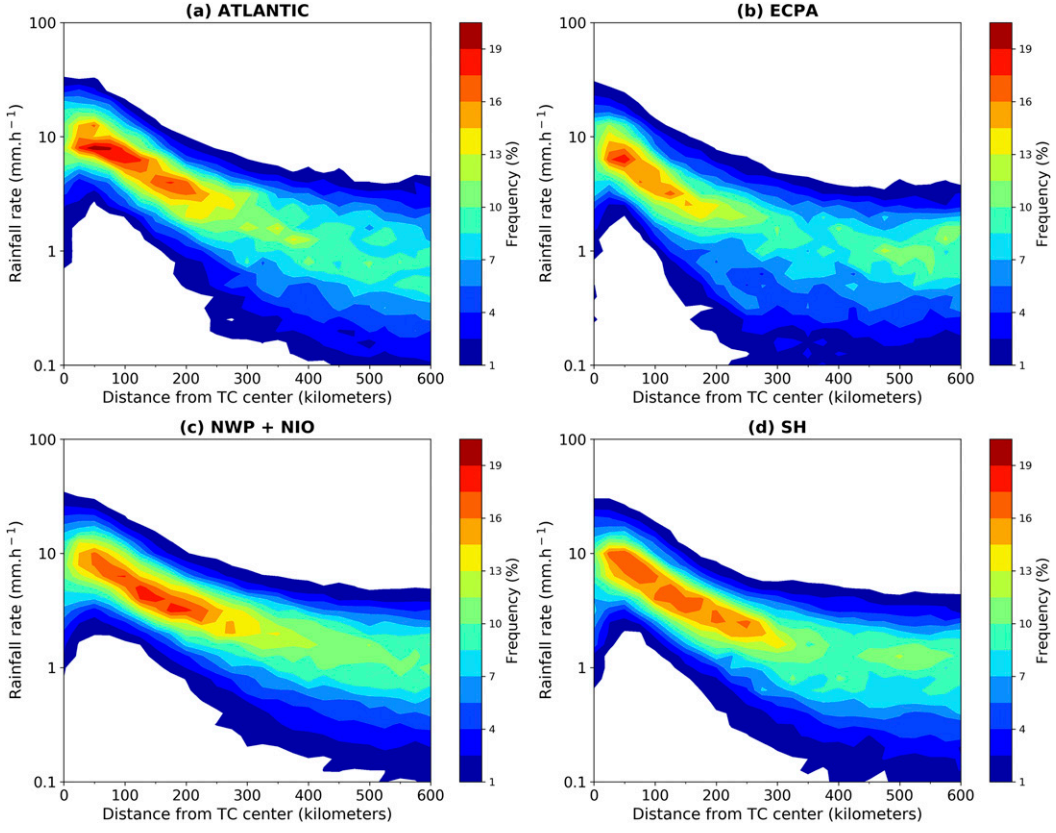

FIG. 3. Radial distribution of rainfall PDFs computed for major hurricanes in the (a) ATL, (b) ECPA, (c) NWP + NIO, and (d) SH basins.

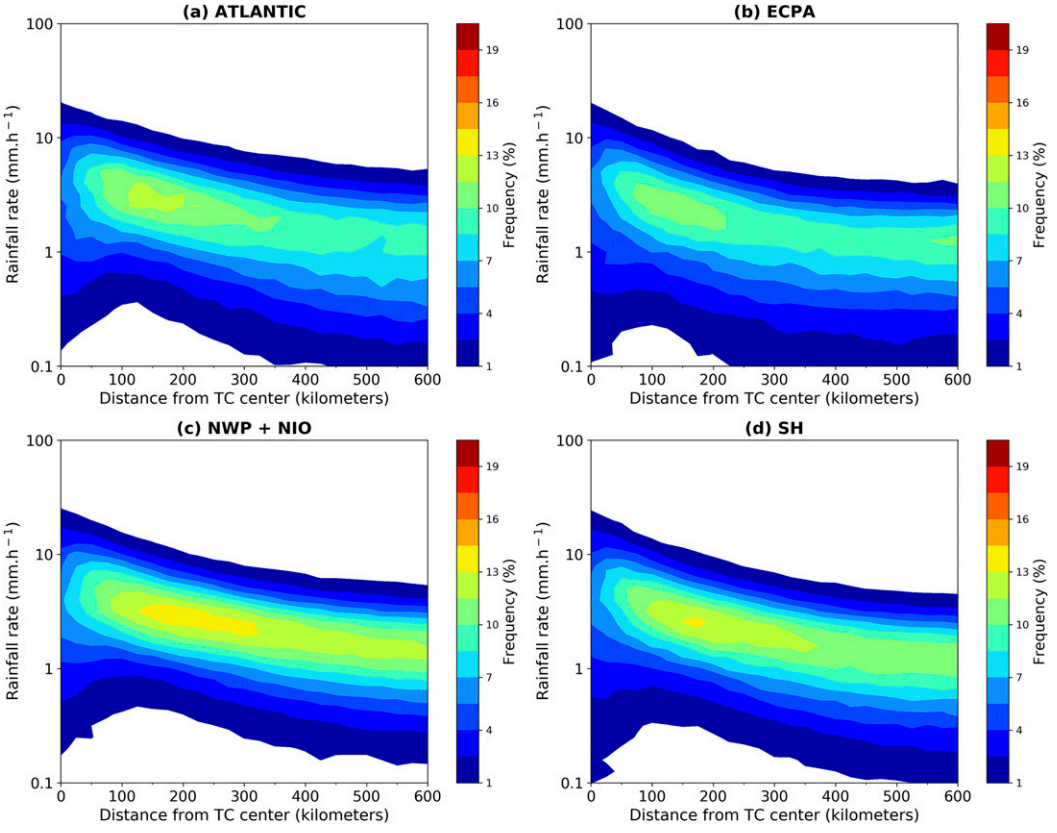

FIG. 4. Radial distribution of rainfall PDFs computed for TCs with intensity less than major hurricanes in the (a) ATL, (b) ECPA, (c) NWP + NIO, and (d) SH basins.

the northwestern Pacific and northern Indian Ocean (NWP + NIO), and the Southern Hemisphere (SH). Note that the NIO basin is combined with the NWP basin due to the small sample size of NIO TCs. TCs in southern Indian Ocean and southern Pacific basins behave similarly in term of the properties studied here and therefore are combined as well. A total of 1789 TCs are analyzed with a sample distribution that consists of 315 in the ATL, 363 in the ECPA, 637 in the NWP + NIO, and 474 in the SPA, respectively (Table 1). Rainfall information is obtained from the multisensor precipitation estimate TRMM and GPM 3B42 (version 7). The 3B42 data provide gridded rainfall information on a 3-h temporal resolution and a 0.25° × 0.25° spatial resolution, covering the latitude band from 50°N to 50°S. Each microwave precipitation estimate is best interpreted as the precipitation rate effective at the nominal observation time (Huffman et al. 2007).

The TC positions, time, and maximum sustained wind speed are obtained from the International Best Track Archive for Climate Stewardship (IBTrACS version 4), which is a global collection of best track data from multiple meteorological agencies to provide a complete global climatology of TCs (Knapp et al. 2018). Only storms in which the 3B42 extent covers the entire inner-core area are considered. To satisfy this condition, we removed those best track positions beyond 46°N and 46°S (approximately 440 km before the edge of the 3B42 border). TCs identified as extratropical were removed using the flags available in columns 23 and 26 of the IBTrACS database. The final dataset includes TCs over both ocean and land. Considering the differences in the reported values from the independent national services working in the Pacific basins, a meticulous cross-check is performed to favor the information from the U.S. Navy's Joint Typhoon Warning Center (JTWC). Regarding intensity categories, based on the definitions in the IBTrACS data, a tropical depression (TD) refers to a system with wind speed from 10 to 33 kt (1 kt ≈ 0.51 m s^{-1}) and a tropical storm (TS) is a system with wind between 34 and 63 kt. The hurricane categories 1 to 5 (CAT1 to CAT5) are adopted from the Saffir–Simpson wind scale.

Variables that characterize the environmental conditions around the storms are obtained from the most recent version of the Statistical Hurricane Intensity Prediction Scheme (SHIPS; last updated July 2018) developmental dataset, which includes 6-h retrievals of observational and derived data of more than 80 TC parameters, including predictions up to 120 h over various annular regions calculated from the TC center (DeMaria and Kaplan 1994, 1999; DeMaria et al. 2005; Schumacher et al. 2013). In the current study, we made an initial selection of 12 SHIPS environmental parameters to be examined: Reynolds sea surface temperature (RSST); wind shear with vortex removed and averaged from 0 to 500 km (SHDC); wind shear

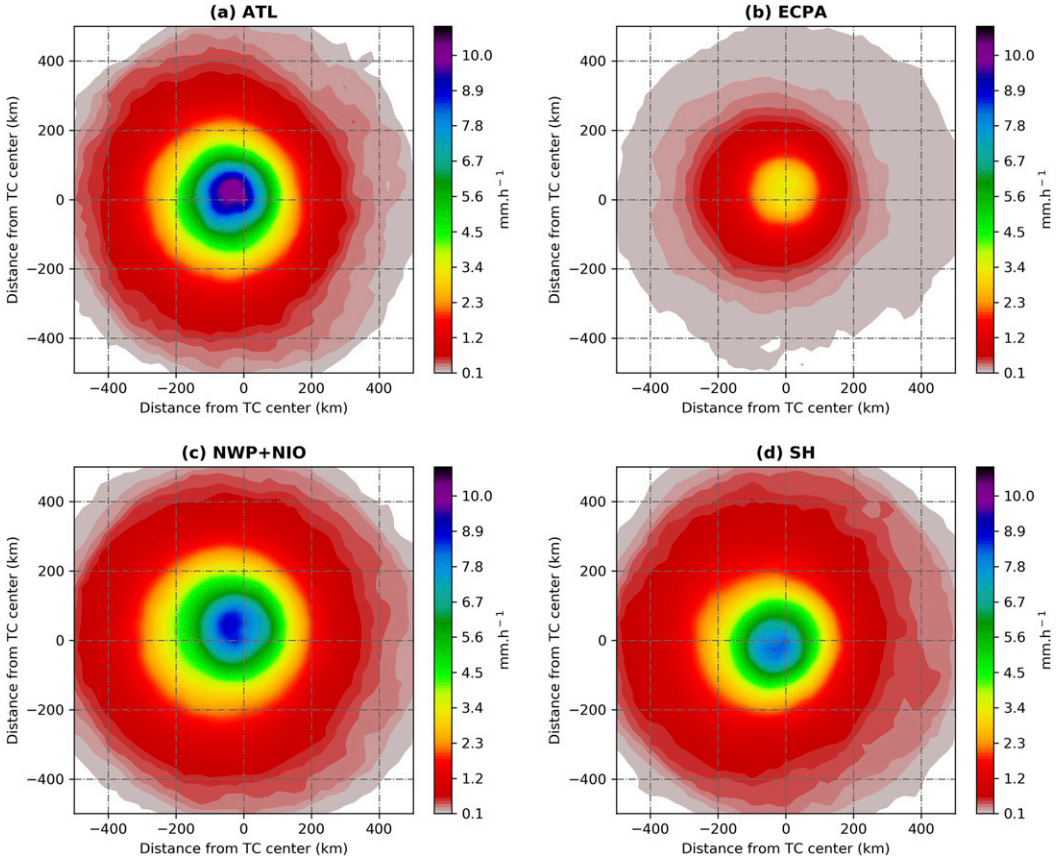

FIG. 5. 2D Composite shear-relative rainfall rate produced by major hurricanes during 1998–2016 in the (a) ATL, (b) ECPA, (c) NWP + NIO, and (d) SH basins. The shear direction is pointing upward.

heading averaged from 0 to 500 km (SHDD); climatological ocean heat content (COHC), average potential temperature (θ_e) difference between a parcel lifted from the surface and its environment with only positive differences considered in the averages (EPOS), which is a parameter similar to the convective available potential energy (CAPE); total precipitable water between 0–200 and 0–500 km (MTPW); relative humidity at three different levels including surface (R000), the 850–700-hPa layer from 200 to 800 km (RHLO), and the 700–500-hPa layer from 200 to 800 km (RHMD); and last, the temperature at both the surface (T000) and the 250-hPa level from 200 to 800 km (T250). Only the values at the initial time ($t = 0$) are employed in our analyses.

b. *Axisymmetric precipitation and 2D plots*

In this study, the radial variation of precipitation is determined by the azimuthal mean rainfall rate in 40 steps of 25-km-wide annuli from the TC center outward to the 600 km, in storm-relative coordinates. This procedure is based on calculating the wavenumber 0 of the Fourier transformation (azimuthal average) as reported in previous investigations (e.g., Lonfat et al. 2004; Chen et al. 2006; Kim et al. 2018). Considering that 25 km is nearly the pixel-size resolution, a scheme in which the map coordinates are assigned to the pixel's center was adopted. Thus, the algorithm only includes pixels when more than half of its size is within the annulus. During the selection of values to consider in the calculations, a threshold of rainfall rates greater than 0.01 mm h^{-1} is used to obtain the averages. The calculation of axisymmetric precipitation is applied to each available record in the combined best track and SHIPS database to examine the radial dependence of TC precipitation as a function of the storm intensity and geographic location (Figs. 1 and 2). As part of the axisymmetric analysis, the radius of maximum azimuthal rain rate (RMR) of each storm is also calculated to allow geometric interbasin comparisons (Fig. 13). The RMR is defined as the radius of the azimuthal mean maximum rainfall within a 400-km radius from the TC center (Shimada et al. 2018); this parameter is extracted as a proxy for the radius of maximum wind. Finally, and to further examine each rainfall rate contribution to the mean values with radial distance, the probability density function (PDF) of rain occurrence in each annulus is determined by classifying the 3B42 rain estimates in equally distributed classes within a logarithm scale. Using the annular PDFs series, contoured frequency by radial distance (CFRD) diagrams are constructed for each basin (Figs. 3 and 4). This procedure is implemented in the same way that Lonfat et al. (2004) and Jiang et al. (2008b) described.

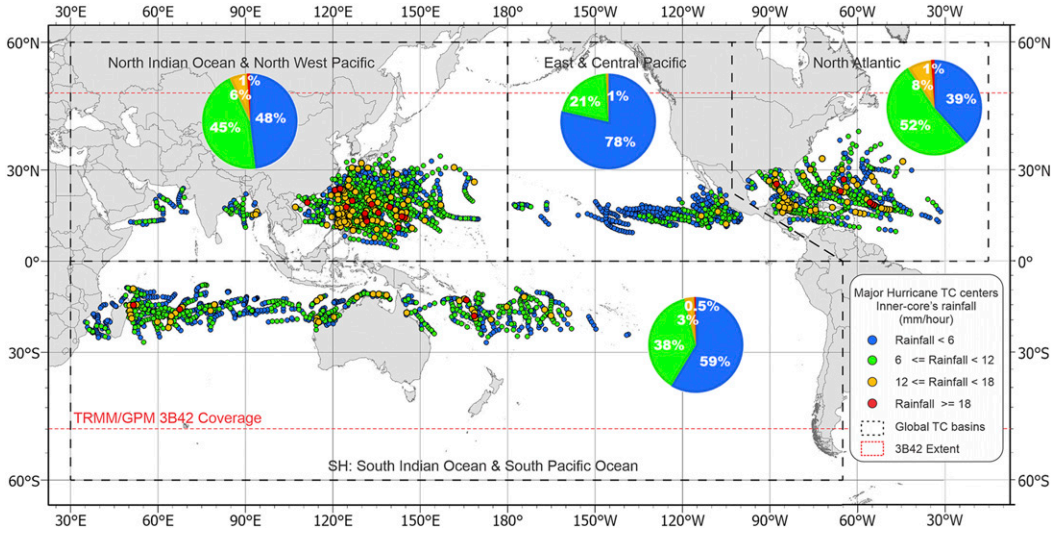

FIG. 6. Global map showing the locations of the centers of major hurricanes for each 3B42 overpass categorized by different mean inner-core rain levels. Pie charts illustrate the percentage of observations for each rainfall rate category in each basin.

In addition to the axisymmetric profiles, bidimensional plots showing the spatial distribution of the composite TC rainfall are created in storm-centered coordinates (Fig. 5). The composite procedure starts from each of the best track positions by selecting the pixels contained in the envelope of a radial buffer from the TC center to 500 km in the 3B42 files. Once obtained, the hurricane-centered grid is rotated along the vertical wind shear vector using the heading values reported in the SHIPS database (variable SDDC). Then, the average rainfall rate is calculated for each cell position in the storm-centered array and categorized by basin.

c. *Mean values, statistical tests, and spatial distribution maps*

The average inner-core rainfall rates are calculated in the region from the TC center to 150 km. In this procedure, we used the same pixel selection rules employed in the algorithm for the azimuthal rainfall rate estimations. To allow comparison through

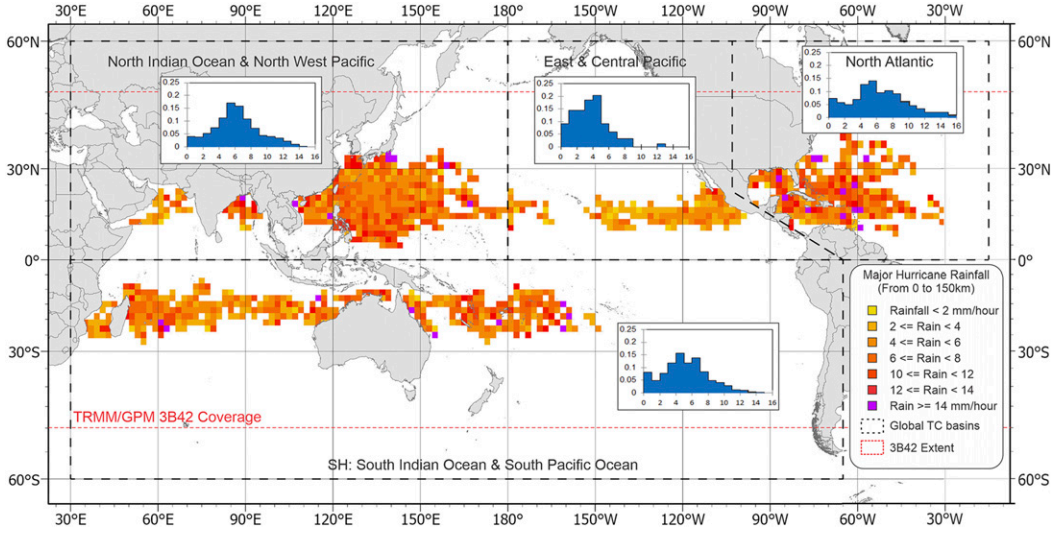

FIG. 7. Map showing the spatial distribution of the normalized TC rainfall produced by major hurricanes in the period 1998–2016 (only the inner-core region is considered). Pixel size is resampled to 2° × 2° for better representation. Histograms show the normalized frequency of inner-core rainfall rate values for each basin.

TABLE 2. Comparison of average inner-core rainfall rate (mm h^{-1}) within 150 km from the TC center for different TC intensity categories and different TC-prone basins in the period 1998–2016. Superscript letters a, b, c, and d denote that the statistical significance of the difference between each basin vs the ATL basin is at the 90%, 95%, 99%, and 99.9% confidence level, respectively. Significance is calculated with respect to Atlantic averages using either a *t* test or Mann–Whitney *U* test, depending on data normality.

Category	ATL	ECPA	NWP + NIO	SH	Global mean	Global mean excluding ATL samples
Tropical depression	2.30	1.95[d]	2.86[d]	2.61[d]	2.51[d]	2.55[d]
Tropical storm	3.18	3.07[b]	4.00[d]	3.46[d]	3.49[d]	3.58[d]
Category 1	4.62	3.72[d]	5.18[d]	4.52	4.64	4.64
Category 2	5.69	3.79[d]	5.93	5.22[d]	5.33[d]	5.27[d]
Category 3	6.42	4.17[d]	6.29[a]	5.58[d]	5.76[d]	5.64[d]
Category 4	7.77	5.32[d]	6.91[d]	6.08[d]	6.61[d]	6.42[d]
Category 5	9.54	6.77[d]	7.98[c]	7.33[d]	7.93[c]	7.72[c]

paired observations with the environmental variables, averaged values are calculated only for those best track records that match with the SHIPS database. Then, the averaged values of the rain and SHIPs variables are categorized by basin. As a second step, a statistical test is used to determine if there is a significant difference for the means of the inner-core rainfall rate values and environmental variables among different basins. The normal distribution of each sample is verified using Shapiro–Wilk normality tests to subsequently apply either a *t* test or a Mann–Whitney *U* test, as required by the statistical normality of the data.

To examine the spatial distribution of inner-core rainfall rates and environmental variables, two types of maps are created: In the first category (Fig. 6; see also Figs. 8–12), point-based maps representing major hurricane centers of each observation are color-coded by intervals of inner-core rainfall rates and environmental variables. Class intervals are initially created using four Jenks' natural breaks in which at least one class is below the global average, and the remaining three are created in the direction of the maximum variation. Once obtained, break limits are rounded to facilitate the map interpretation. In the second category (Fig. 7), a continuous map showing normalized accumulation of inner-core rainfall is created from the 3B42 data. The normalized values result from the ratio between the total accumulated rain and the number of samples at each geographic location. Finally, the resulting map is resampled to a 2° × 2° grid and then color-coded using the same approach of the point-based maps, but for a higher number of intervals.

3. Results

a. *Axisymmetric findings*

Figure 1 shows the radial distribution of azimuthally average rainfall rates stratified by geographic location and intensity categories. In all the cases, there is a positive relationship between TC intensity and the precipitation rate, which is more evident in the region within the first 300 km from the TC center. In the region from 300 to 550 km, rainfall rates uniformly decrease outward to 1 mm h^{-1}, and in the case of the area beyond 550 km, the rainfall rate tends to be nearly the same for all the TC intensity categories. In general, mean rainfall rates increase with the storm intensity at all radii. The shorter the distance from the TC center, the higher the rainfall rates, except for the annuli associated with the storm's eye.

Globally, TDs and TSs exhibit their maximum rainfall rate in the vicinity of their geometric center, in an intensity interval between 3 and 4 mm h^{-1}. In contrast, CAT1 to CAT5 storms show their peaks between 6 and 10.7 mm h^{-1}, ranging from 50 to 70 km from the TC center. However, the Atlantic basin exhibits more pronounced rainfall rates in the inner-core region (Fig. 1a), mainly within major hurricane categories (CAT3–CAT5). At their peak, Atlantic rates differ from the global average rates by +6.4%, +13.9%, and +18.8% for CAT3, CAT4, and CAT5, respectively.

The same pattern appears in the mean inner-core rainfall rates summarized in Table 2. It can be seen that for major hurricanes, the Atlantic basin produces heavier inner-core rainfall than other basins, and its rainfall rate surpasses the global averages. Results of the *t* test and Mann–Whitney *U* test indicate that there is a significant difference between the mean values of the Atlantic with respect to the other basins. In all the major hurricane cases, the statistical significance difference exceeds 90%, and for CAT4 and CAT5 significance values range from 99% to 99.9% in all the interbasin comparisons.

Figure 2 shows the differences in the mean radial profiles between major hurricanes and the rest of the intensity categories; these axisymmetric profiles confirm the presence of

TABLE 3. Number and percentage of major hurricane observations in different inner-core mean rain rate categories.

Variable	ATL	ECPA	NWP + NIO	SH	Total
Inner-core rain < 6 mm h^{-1}	223 (38.4%)	414 (78.6%)	865 (48.1%)	639 (58.6%)	2141 (53.6%)
6–12 mm h^{-1}	304 (52.3%)	109 (20.7%)	808 (44.9%)	410 (37.6%)	1631 (40.8%)
12–18 mm h^{-1}	48 (8.3%)	4 (0.8%)	108 (6.0%)	36 (3.3%)	196 (4.9%)
>18 mm h^{-1}	6 (1.0%)	0	17 (0.9%)	5 (0.5%)	28 (0.7%)
Total of 3B42 observations for major hurricanes	581	527	1798	1090	3996

TABLE 4. Mean value of inner-core rain, VMAX, and environmental variables of major hurricanes during 1998–2016 in different basins. Superscript letters a, b, c, and d denote that the statistical significance of the difference between each basin vs the ATL basin is at the 90%, 95%, 99%, and 99.9% confidence level, respectively. Significance is calculated with respect to Atlantic averages using either a *t* test or Mann–Whitney *U* test, depending on data normality.

Variable	ATL	ECPA	NWP + NIO	SH	Global mean	Global mean excluding ATL samples
Mean rainfall rate within 150 km (mm)	7.28	4.63^{d}	6.78^{d}	5.95^{d}	6.34^{d}	6.18^{d}
VMAX (kt)	115.66	112.98^{d}	118.06^{c}	114.4^{a}	116.05	116.12
SHDC (m s^{-1})	11.67	8.27^{d}	10.37^{d}	12.45	10.85^{c}	10.71^{d}
EPOS (°C)	11.08	7.45^{d}	10.03^{d}	8.38^{d}	9.39^{d}	9.10^{d}
RHLO (%)	70.27	72.98^{d}	75.51^{d}	75.21^{d}	74.33^{d}	75.02^{d}
RHMD (%)	58.07	63.92^{d}	64.93^{d}	62.38^{d}	63.10^{d}	63.96^{d}
T250 (°C)	−40.22	−39.93^{d}	−37.93^{d}	−38.81^{d}	−38.76^{d}	−38.52^{d}

geographical variations of rainfall rates from basin to basin. On the one hand, major hurricanes exhibit an ascending sequence of rainfall intensity that begins with ECPA, followed by SH and NWP + NIO, and finishing with ATL as the basin with the heaviest rainfall rate. This intensity order is preserved across the inner-core region but changes beyond 150–175 km from the TC center, where NWP + NIO starts to exhibit the highest rainfall rates (Fig. 2a). On the other hand, TD, TS, and minor hurricanes show a different ascending order in the basin intensities. In their case, the sequence begins with ECPA, followed by SH and ATL, and finishing with NWP + NIO. However, Atlantic TCs reduce their rainfall rates below the SH averages in the inner-core region (Fig. 2b).

Figures 3 and 4 show the rain-rate frequency distributions with radial distance computed outward to the 600-km radius from the TC center. Figure 3 focuses on the frequencies for major hurricanes across different basins. Within the 50–200-km radius, distributions are relatively narrow, with values more concentrated around the mode and short symmetrical tails (i.e., little to no skewness and a modest leptokurtic pattern). Beyond 200 km the distribution broadens, becoming left-tailed with the mean and mode in direction to the highest rainfall rates. Interbasin comparison shows that Atlantic storms have more occurrences of high inner-core rainfall rate values within the first 150 km than other global basins (Fig. 3a), reaching precipitation rates near 8–11 mm h^{-1} with frequencies above 17%. This basin also exhibits more frequent events surpassing 10 mm h^{-1}. NWP + NIO and ECPA reveal relatively similar PDFs in the region between 50 and 300 km, except for a more pronounced mode around 150 km. ECPA storms show high frequency in the first 150 km but a broader expansion of rainfall rates beyond this range. In contrast with the notable variations observed in major hurricanes, Fig. 4 shows that TD, TS, and minor hurricanes have more homogeneous PDFs in the inner core, although they exhibit slightly higher frequencies in the region from 150 to 300 km, especially in the NWP + NIO and SH basins.

Two-dimensional plots shown in Fig. 5 describe the distribution of rainfall rates for major hurricanes across different basins in storm-centered coordinates, with the shear direction

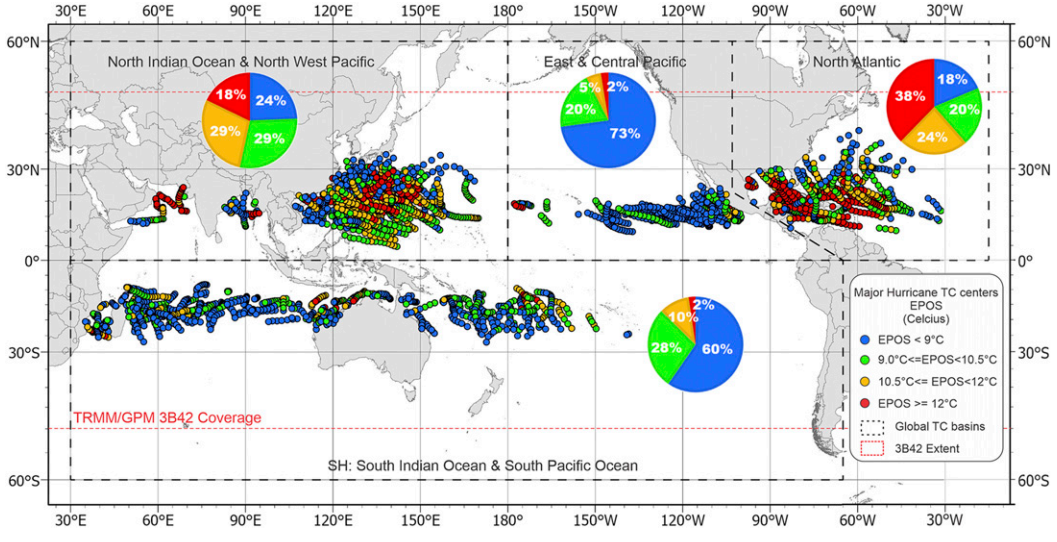

FIG. 8. Global map showing the centers of major hurricanes for each SHIPS data point categorized by different EPOS levels. Pie charts illustrate the percentage of observations for each EPOS category in each basin.

TABLE 5. Number and percentage of major hurricane observations in different categories of EPOS.

Variable	ATL	ECPA	NWP + NIO	SH	Total
EPOS < 9°C	108 (18.6%)	384 (72.9%)	439 (24.4%)	650 (59.6%)	1581 (39.6%)
9.0°–10.5°C	116 (20.0%)	104 (19.7%)	521 (29.0%)	302 (27.7%)	1043 (26.1%)
10.5°–12.0°C	138 (23.8%)	26 (4.9%)	517 (28.8%)	113 (10.4%)	794 (19.9%)
EPOS >12°C	219 (37.7%)	13 (2.5%)	321 (17.9%)	25 (2.3%)	578 (14.5%)
Total of 3B42 observations for major hurricanes	581	527	1798	1090	3996

pointing upward. In concordance with observational and modeling studies (e.g., Cecil 2007; Wingo and Cecil 2010), this plot shows that rainfall is favored in the downshear direction and also to the left to the shear vector in the Northern Hemisphere, and upshear-right for those storms occurring in the Southern Hemisphere. These plots confirm the presence of geographical variations of rainfall rates on a basin basis, in which major hurricanes exhibit an ascending sequence of rainfall intensity that begins with ECPA as the weakest (Fig. 5b), followed by SH (Fig. 5d) and NWP + NIO (Fig. 5c), and finishing with ATL as the basin with the heaviest rainfall rate (Fig. 5a).

b. *Geographic distribution of major hurricane precipitation*

Figure 6 shows the spatial distribution of major hurricane centers along global basins. In this map, the frequency and TC center positions are color-coded for four different mean inner-core rain categories. It can be observed that rainfall rates below 6 mm h^{-1} are dominant in all basins except for the Atlantic, where the most frequent rates oscillate in the range from 6 to 12 mm h^{-1}. Similar patterns can be found along the 6–12, 12–18, and >18 mm h^{-1} intervals, in which the pattern of heavier inner-core rains in the Atlantic basin appears systematically. Table 3 summarizes the number and percentage of observations that match with Fig. 6. Here, the percentage of the number of events with more intense precipitation is higher in the Atlantic basin. Considering that the most representative percentage differences occur in the lower intervals (i.e., not in the most extreme events), we discard the hypothesis that unusual events are the cause that produces these differences.

Figure 7 illustrates the spatially normalized TC rainfall produced by the inner core in a 2° gridded representation at a global scale. In this map, the places with the heavier precipitation in the inner core are easily distinguishable (red and magenta). Although an important number of these locations follow random patterns, it can be observed that some of the rainiest places are collocated over sectors of well-recognized oceanic warm currents. In the particular case of the Atlantic basin, the rainiest events (greater than 14 mm h^{-1}) appear clustered across two branches: the first branch flows north and east of the West Indies, nearly along the 60°W parallel, and the second flows into the Caribbean Sea following the Caribbean and the Gulf of Mexico currents. This map also shows the histograms that describe the distribution of pixel values in each basin. It can be seen that whereas the NWP + NIO basin has a normally

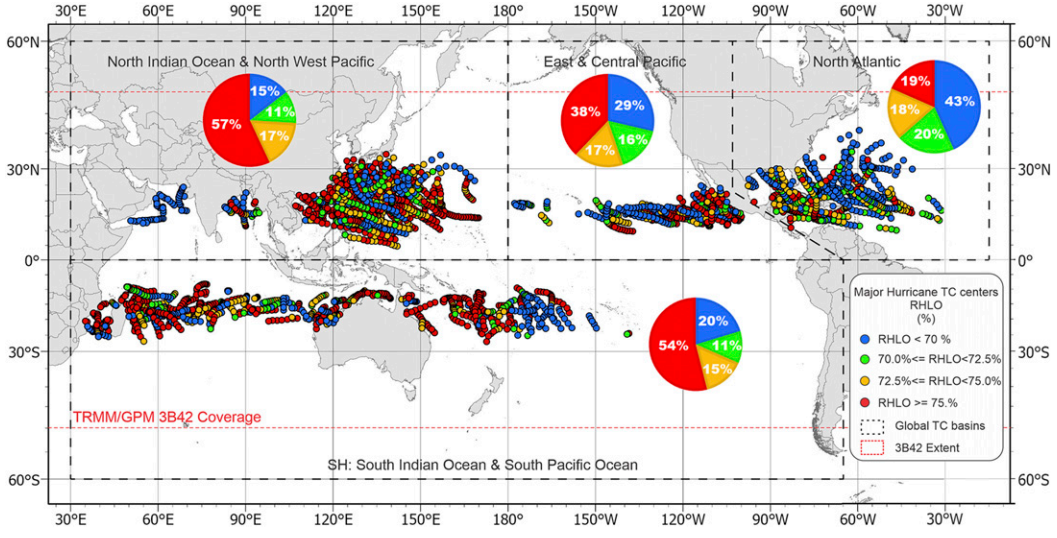

FIG. 9. Global map showing the locations of the centers of major hurricanes for each SHIPS data point categorized by different RHLO levels. Pie charts illustrate the percentage of observations for each RHLO category in each basin.

TABLE 6. Number and percentage of major hurricane observations in different categories of RHLO.

Variable	ATL	ECPA	NWP + NIO	SH	Total
RHLO < 70%	251 (43.2%)	151 (28.7%)	261 (14.5%)	222 (20.4%)	885 (22.1%)
70.0%–72.5%	118 (20.3%)	85 (16.1%)	206 (11.5%)	122 (11.2%)	531 (13.3%)
72.5%–75.0%	105 (18.1%)	91 (17.3%)	307 (17.1%)	158 (14.5%)	661 (16.5%)
RHLO > 75.0%	107 (18.4%)	200 (38.0%)	1024 (57.0%)	588 (53.9%)	1919 (48.0%)
Total of 3B42 observations for major hurricanes	581	527	1798	1090	3996

distributed histogram, SH, ECPA, and ATL follow skewed distributions. For instance, ECPA exhibits more frequency of lighter rainfall events, and ATL and SH observe histograms tailed to the right, in which the Atlantic storms reach heavier rainfall rates.

c. *Environmental parameters around major hurricanes*

As one of the potential causes to explain the heavier inner-core rainfall rates in the Atlantic basins, some environmental variables available in the SHIPS developmental database are examined (see the discussion in section 4). As the first step, an initial selection of 12 variables was considered. However, we discarded most of them after performing a significance test of the difference between each basin's mean values with reference to mean values in the ATL basin. Table 4 shows the final selection of environmental variables along with their corresponding levels of significance. It can be observed that ATL exhibits the lowest values of RHLO, RHMD, and T250. Likewise, ATL shows the highest EPOS globally and shear values in the Northern Hemisphere.

Based on the above result, further analysis on the statistical and spatial distribution of the differences is performed. Thus, Fig. 8 and Table 5 show that EPOS greater than 12°C presents higher occurrence in the Atlantic basin (37%), more than double than in other global basins. In terms of spatial distribution, the highest EPOS values in ATL are fairly collocated with the highest rainfall rates shown in Figs. 6 and 7. Interestingly, EPOS in this interval shows little spatial correlation with the maximum rainfall rates in the other basins.

Regarding relative humidity differences, Fig. 9 and Table 6 show that RHLO below 70% is the most dominant feature in ATL. On the contrary, values above 75% are the most frequent in other basins. ATL also exhibits the most frequent intermediate intervals of RHLO in the range from 70% to 75%. Likewise, identical patterns occur with RHMD (Fig. 10 and Table 7) in which drier environments appear more commonly in the Atlantic basin, particularly in storms with RHMD below 60%. From the spatial perspective, it is difficult to establish well-defined patterns to link the highest precipitation rates with relative humidity differences. However, by contrasting Fig. 7 with Figs. 9 and 10, it can be seen that relative humidity contributes differently to the production of rainfall in the Atlantic basin. For instance, while ECPA storms seem to be favored by the moister environment, the Atlantic seems favored by slightly drier conditions below the global averages.

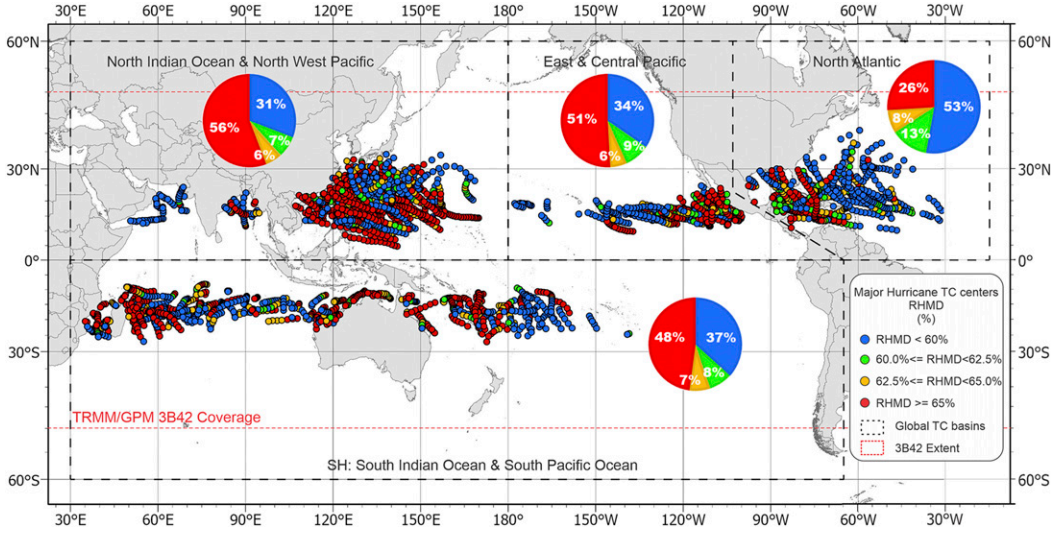

FIG. 10. Global map showing the locations of the centers of major hurricanes for each SHIPS data point categorized by different RHMD levels. Pie charts illustrate the percentage of observations for each RHMD category in each basin.

TABLE 7. Number and percentage of major hurricane observations in different categories of RHMD.

Variable	ATL	ECPA	NWP + NIO	SH	Total
RHMD < 60%	307 (52.8%)	182 (34.5%)	555 (30.9%)	400 (36.7%)	1444 (36.1%)
60.0%–62.5%	76 (13.1%)	46 (8.7%)	134 (7.5%)	89 (8.2%)	345 (8.6%)
62.5%–65.0%	47 (8.1%)	31 (5.9%)	106 (5.9%)	79 (7.2%)	263 (6.6%)
RHLO > 65.0%	151 (26.0%)	268 (50.9%)	1003 (55.8%)	522 (47.9%)	1944 (48.6%)
Total of 3B42 observations for major hurricanes	581	527	1798	1090	3996

About wind shear, Fig. 11 and Table 8 show that the Atlantic has the highest frequency of storms above 11 and 12 m s^{-1}, with a relatively similar distribution to the trend observed in the SH. In contrast, ECPA shows its highest frequency in environments with wind shear in the lowest interval below 10 m s^{-1}. NWP + NIO reveals a behavior in between. Spatially, wind shear values are slightly stronger poleward in all basins, following a random pattern with little collocation to the heaviest rainfall rates. Finally, Fig. 12 and Table 9 show that the most predominant temperatures at 250 hPa in the Atlantic basin occur below −40°C. Interestingly, NWP + NIO has the opposite frequency distribution in each interval.

4. Discussion

Previous interbasin comparisons of azimuthal mean rain rates suggest that the main differences occur around the inner-core region. For instance, Lonfat et al. (2004) found that TCs in the NIO show larger rain rates than other basins within the inner 100-km radius, while ECPA TCs have less rain in the 250–350-km zone. In that study, the authors reported potential uncertainties due to the small number of samples and suggested that interbasin differences could be associated with the interactions between the TC and its environment.

Our results, using 19-yr satellite data, show that interbasin differences can be found in the region up to 550 km from the TC center, with the most significant variations in the first 300 km and the inner-core region (0–150 km). However, for the first time in the literature, we found that in the inner core, the Atlantic basin exhibits larger rainfall rates than other basins, particularly for the most intense TCs. This result contradicts previous interbasin comparison results using shorter time series by Lonfat et al. (2004). Three main possible hypotheses may explain the Atlantic difference: 1) this variation could be explained by geometrical differences (e.g., size or area) between Atlantic hurricanes and those occurring in other basins; 2) variation could be the result of differential TC intensities in this basin with respect to the others; and/or 3) differences in the interactions between TCs and their environment may favor the increase of rainfall in this basin.

Concerning the first hypothesis, we computed the average RMR for the different global basins seeking size-related differences. Figure 13 shows the resulting RMRs categorized

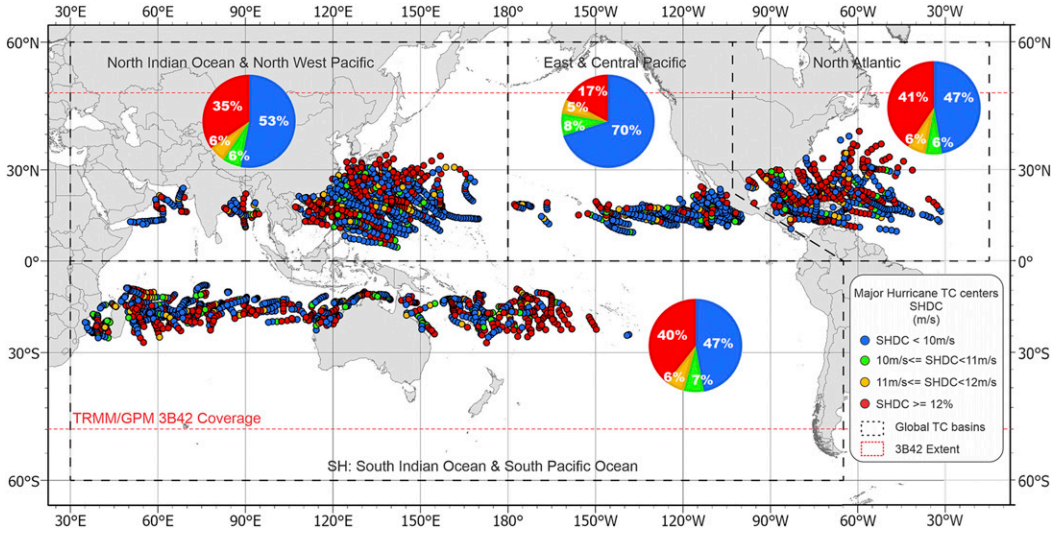

FIG. 11. Global map showing the locations of the centers of major hurricanes for each SHIPS data point categorized by different SHDC levels. Pie charts illustrate the percentage of observations for each SHDC category in each basin.

TABLE 8. Number and percentage of major hurricane observations in different categories of SHDC.

Variable	ATL	ECPA	NWP + NIO	SH	Total
SHDC $< 10\,m\,s^{-1}$	275 (47.3%)	369 (70.0%)	952 (52.9%)	514 (47.2%)	2110 (52.8%)
10.0–11.0 $m\,s^{-1}$	33 (5.7%)	41 (7.8%)	118 (6.6%)	76 (7.0%)	268 (6.7%)
11.0–12.0 $m\,s^{-1}$	37 (6.4%)	26 (4.9%)	104 (5.8%)	70 (6.4%)	237 (5.9%)
SHDC $> 12.0\,m\,s^{-1}$	236 (40.6%)	91 (17.3%)	624 (34.7%)	430 (39.4%)	1381 (34.6%)
Total of 3B42 observations for major hurricanes	581	527	1798	1090	3996

by basin and TC intensity. As expected, most of the samples in central and eastern Pacific hurricanes show the shortest RMRs and northwestern Pacific the largest. In this analysis, Atlantic hurricanes exhibit an intermediate behavior, almost identical to the global average shown in Fig. 13a. Therefore, a geometrical difference is an improbable reason to explain the wetter CAT3 to CAT5 hurricanes occurring in the Atlantic basin.

To test the second hypothesis, the average values of the maximum sustained wind speed are calculated and stratified by both TC intensity and geographic location. Table 4 shows that major hurricanes in NWP + NIO have the highest mean value of maximum sustained wind among all global basins. In these calculations, the Atlantic basin presents an intermediate behavior compared to the other basins. Therefore, the second hypothesis is also an improbable cause of the wetter major hurricanes occurring in the Atlantic basin.

The third hypothesis seeks an explanation based on the environmental interactions of TC occurring in the Atlantic basin relative to those present in other basins. Based on the results shown in Tables 3–9, we believe that the drier environment in the low- to middle-level troposphere (RHLO and RHMD) and colder air temperature at the upper level (T250) could induce a larger instability. Considering that under the presence of unstable air, low relative humidity, and low T250 convection activity is highly promoted, our results indicate that ATL has more favorable environmental conditions associated with major hurricanes to produce convective rainfall in the inner-core region. This interpretation is ratified by the higher value of EPOS, and therefore a higher value of CAPE, in ATL major hurricanes when compared to the other global basins. For this reason, we hypothesize that stronger convection is the main contributor to producing wetter inner-core conditions. This proposition is supported by the theory behind the classic hurricane models (e.g., Emanuel 1986) that explain the release of energy through a moist adiabatic expansion that converts stored latent heat into sensible heat in an environment with higher potential buoyancy than its surrounding environment. In other words, in the presence of higher CAPE, hurricanes tend to produce more precipitation.

With regard to the influence of environmental vertical wind shear (SHDC), Tables 4 and 8 show that the ATL basin has slightly higher shear magnitudes associated with major hurricanes than other basins in the Northern Hemisphere. It is well known that a weak vertical shear is a necessary condition for

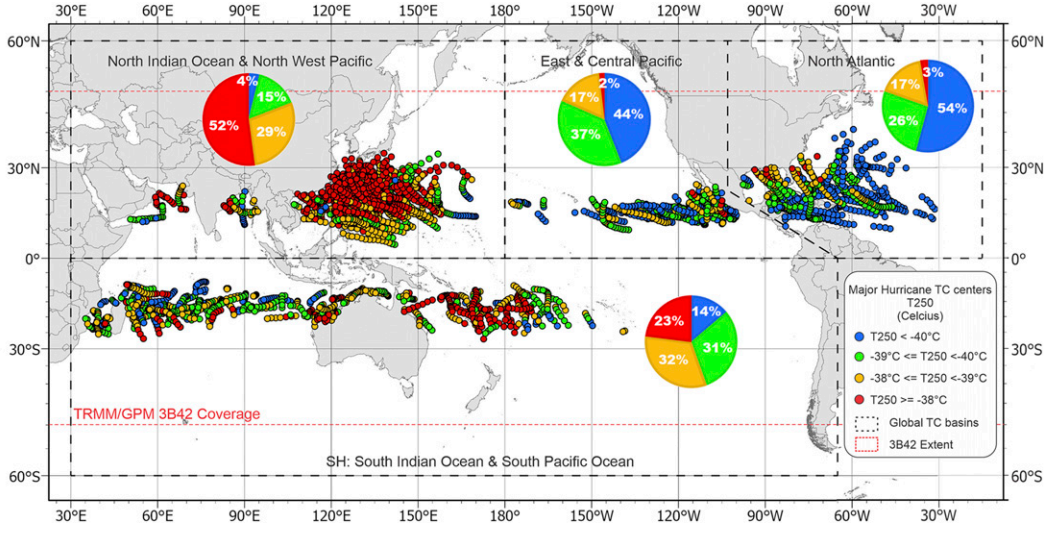

FIG. 12. Global map showing the locations of the centers of major hurricanes for each SHIPS data point categorized by different T250 levels. Pie charts illustrate the percentage of observations for each T250 category in each basin.

TABLE 9. Number and percentage of major hurricane observations in different categories of T250.

Variable	ATL	ECPA	NWP + NIO	SH	Total
T250 < −40°C	315 (54.2%)	232 (44.0%)	69 (3.8%)	150 (13.8%)	766 (19.2%)
From −39.0° to −40.0°C	152 (26.2%)	198 (37.6%)	275 (15.3%)	336 (30.8%)	961 (24.0%)
From −38.0° to −39.0°C	99 (17.0%)	88 (16.7%)	517 (28.8%)	353 (32.4%)	1057 (26.5%)
T250 > −38°C	15 (2.6%)	9 (1.7%)	937 (52.1%)	251 (23.0%)	1212 (30.3%)
Total of 3B42 observations for major hurricanes	581	527	1798	1090	3996

TC development. However, multiple studies also have demonstrated that when TCs interact with moderate amounts of wind shear, convection can be promoted, and TCs often take an asymmetric structure that leads to rainfall enhancement over favored sectors of the TC structure (Corbosiero and Molinari 2002; Lonfat et al. 2004; Cecil 2007; Pei and Jiang 2018). Specifically, Molinari and Vollaro (2010a,b) showed that highly sheared TCs produced 30% larger average CAPE versus relatively unsheared TCs through the asymmetric process. Therefore, the higher shear condition for ATL major hurricanes is favorable for stronger convection, and thus heavier inner-core rain rates than major hurricanes in other Northern Hemisphere basins.

5. Conclusions

Using 19 years of TRMM and GPM 3B42 rainfall data for TCs, it is found that major (CAT3 to CAT5) hurricanes in the ATL basin have significantly larger mean rainfall rates in the inner-core region than those in all other TC-prone basins. At the peak rainfall value in the inner core, the composite rainfall rate of major hurricanes in the ATL basin is higher than the global average by 6.4%, 13.9%, and 18.8% for CAT3, CAT4, and CAT5 hurricanes, respectively.

To determine which atmospheric conditions were most likely responsible for the heavier rainfall rates in this basin, we tested three hypotheses: 1) geometrical differences, 2) differential TC wind speed intensity, and 3) special environmental conditions through the analysis of the SHIPS developmental database. Our results indicate that particular environmental conditions could explain this difference. We found that major hurricane in the ATL basin are associated with lower relative humidity in the low to middle level, lower upper-level temperature, higher CAPE, and higher vertical wind shear magnitude in the environment. It is the general understanding that drier condition above the surface with lower upper-level temperature could promote convective instability, indicating by the higher CAPE values. Our results are consistent with previous studies showing that higher ambient shear could promote higher CAPE, and therefore strong convection and heavier rain (Molinari and Vollaro 2010a,b). Based on these results, it is suggested that the heavier inner-core rain in major hurricanes in the Atlantic basin is mainly associated with drier relative humidity in the low to middle troposphere, colder air temperature at upper levels, higher CAPE, and stronger vertical wind shear than major hurricanes in other basins.

It is clear that the above findings are merely from the observational perspective through the examination of composite satellite rainfall observations and SHIPS environmental parameter analyses. A detailed examination of the mechanisms that produce heavier inner-core rainfall rates in major hurricanes in the Atlantic basin must be addressed from the modeling perspective to establish detailed causal linkages and

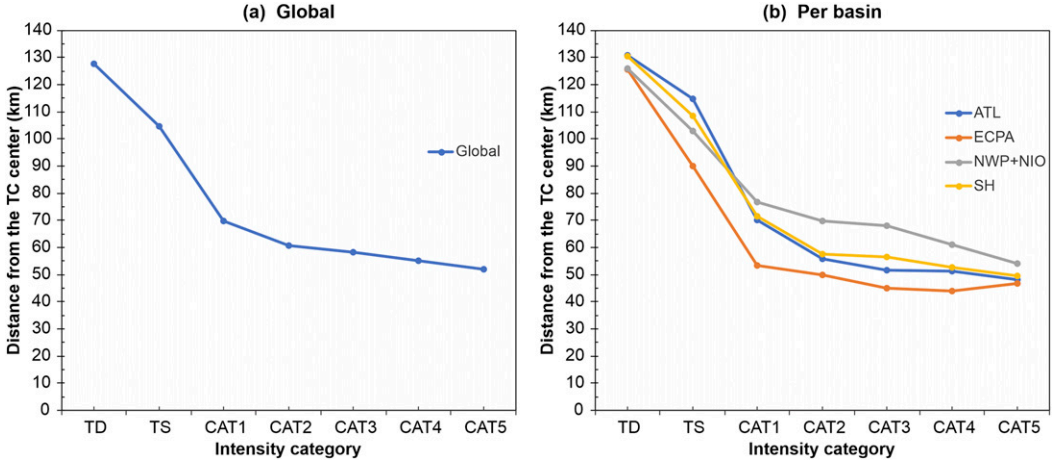

FIG. 13. RMR as a function of TC intensity (a) for all global TCs and (b) for four different basins.

refine our understanding of the peculiarities observed in this basin. Future work will include analyzing additional environmental parameters from model reanalysis data to examine the influence of spatial distribution of these parameters on TC rain intensity. Another interesting point is that this study found that Atlantic TCs with intensity lower than major hurricane strength have weaker inner-core rain than those in other basins. Future study will be done to explore why the rainfall difference exists between weaker and stronger TCs in the Atlantic. The advent of new and more detailed information sources will contribute to the future improvement of this topic.

Acknowledgments. This research is part of the first author's Ph.D. study. The first author was supported by the Fulbright-Colciencias grant as part of the cultural exchange program between the United States of America and the Republic of Colombia. As the PI, the second author would like to thank the following funding support: NSF Grant 1947304 under the direction of Dr. Jielun Sun, NASA Weather And Atmospheric Dynamics (WAAD) Grant NNX17AH72G under the direction of Drs. Ramesh Kakar and Gail Jackson, and NOAA Joint Hurricane Testbed (JHT) Grant NA17OAR4590142 under the direction of Mr. Richard Fulton. We thank the two anonymous reviewers and the editor Dr. Baoqiang Xiang for their helpful comments, which lead to substantial improvement of the manuscript.

REFERENCES

Biswas, M., and Coauthors, 2017: Hurricane Weather Research and Forecasting (HWRF) Model: 2017 scientific documentation. NCAR Tech. Note NCAR/TN-544+STR, 99 pp., https://doi.org/10.5065/D6MK6BPR.

Cecil, D. J., 2007: Satellite-derived rain rates in vertically sheared tropical cyclones. *Geophys. Res. Lett.*, **34**, L02811, https://doi.org/10.1029/2006GL027942.

Chen, S. S., J. A. Knaff, and F. D. Marks, 2006: Effects of vertical wind shear and storm motion on tropical cyclone rainfall asymmetries deduced from TRMM. *Mon. Wea. Rev.*, **134**, 3190–3208, https://doi.org/10.1175/MWR3245.1.

Corbosiero, K. L., and J. Molinari, 2002: The effects of vertical wind shear on the distribution of convection in tropical cyclones. *Mon. Wea. Rev.*, **130**, 2110–2123, https://doi.org/10.1175/1520-0493(2002)130<2110:TEOVWS>2.0.CO;2.

DeMaria, M., and J. Kaplan, 1994: A Statistical Hurricane Intensity Prediction Scheme (SHIPS) for the Atlantic basin. *Wea. Forecasting*, **9**, 209–220, https://doi.org/10.1175/1520-0434(1994)009<0209:ASHIPS>2.0.CO;2.

——, and ——, 1999: An updated Statistical Hurricane Intensity Prediction Scheme (SHIPS) for the Atlantic and eastern North Pacific basins. *Wea. Forecasting*, **14**, 326–337, https://doi.org/10.1175/1520-0434(1999)014<0326:AUSHIP>2.0.CO;2.

——, M. Mainelli, L. K. Shay, J. A. Knaff, and J. Kaplan, 2005: Further improvements to the Statistical Hurricane Intensity Prediction Scheme (SHIPS). *Wea. Forecasting*, **20**, 531–543, https://doi.org/10.1175/WAF862.1.

Emanuel, K.A., 1986: An air–sea interaction theory for tropical cyclones. Part I: Steady-state maintenance. *J. Atmos. Sci.*, **43**, 585–604, https://doi.org/10.1175/1520-0469(1986)043<0585:AASITF>2.0.CO;2.

Ferraro, R., and Coauthors, 2005: The tropical rainfall potential (TRaP) technique. Part II: Validation. *Wea. Forecasting*, **20**, 465–475, https://doi.org/10.1175/WAF861.1.

Huffman, G. J., and Coauthors, 2007: The TRMM multi-satellite precipitation analysis (TMPA): Quasi-global, multiyear, combined-sensor precipitation estimates at fine scales. *J. Hydrometeor.*, **8**, 38–55, https://doi.org/10.1175/JHM560.1.

Jiang, H., and E. J. Zipser, 2010: Contribution of tropical cyclones to the global precipitation from eight seasons of TRMM data: Regional, seasonal, and interannual variations. *J. Climate.*, **23**, 1526–1543, https://doi.org/10.1175/2009JCLI3303.1.

——, J. B. Halverson, and E. J. Zipser, 2008a: Influence of environmental moisture on TRMM-derived tropical cyclone precipitation over land and ocean. *Geophys. Res. Lett.*, **35**, L17806, https://doi.org/10.1029/2008GL034658.

——, ——, J. Simpson, and E. J. Zipser, 2008b: Hurricane "rainfall potential" derived from satellite observations aids overland rainfall prediction. *J. Appl. Meteor. Climatol.*, **47**, 944–959, https://doi.org/10.1175/2007JAMC1619.1.

Kidder, S. Q., J. A. Knaff, S. J. Kusselson, M. Turk, R. R. Ferraro, and R. J. Kuligowski, 2005: The tropical rainfall potential (TRaP) technique. Part I: Description and examples. *Wea. Forecasting*, **20**, 456–464, https://doi.org/10.1175/WAF860.1.

Kim, D., C. Ho, D. R. Park, J. C. Chan, and Y. Jung, 2018: The relationship between tropical cyclone rainfall area and environmental conditions over the subtropical oceans. *J. Climate*, **31**, 4605–4616, https://doi.org/10.1175/JCLI-D-17-0712.1.

Knapp, K. R., H. J. Diamond, J. P. Kossin, M. C. Kruk, C. J. Schreck, 2018: International Best Track Archive for Climate Stewardship (IBTrACS) project, version 4. Subset from 1998 to 2016. NOAA National Centers for Environmental Information, accessed 10 July 2019, https://doi.org/10.25921/82ty-9e16.

Lin, Y., M. Zhao, and M. Zhang, 2015: Tropical cyclone rainfall area controlled by relative sea surface temperature. *Nat. Commun.*, **6**, 6591, https://doi.org/10.1038/ncomms7591.

Lonfat, M., F. D. Marks, and S. S. Chen, 2004: Precipitation distribution in tropical cyclones using the Tropical Rainfall Measuring Mission (TRMM) Microwave Imager: A global perspective. *Mon. Wea. Rev.*, **132**, 1645–1660, https://doi.org/10.1175/1520-0493(2004)132<1645:PDITCU>2.0.CO;2.

——, R. Rogers, T. Marchok, and F. D. Marks Jr., 2007: A parametric model for predicting hurricane rainfall. *Mon. Wea. Rev.*, **135**, 3086–3097, https://doi.org/10.1175/MWR3433.1.

Molinari, J., and D. Vollaro, 2010a: Distribution of helicity, CAPE, and shear in tropical cyclones. *J. Atmos. Sci.*, **67**, 274–284, https://doi.org/10.1175/2009JAS3090.1.

——, and ——, 2010b: Rapid intensification of a sheared tropical storm. *Mon. Wea. Rev.*, **138**, 3869–3885, https://doi.org/10.1175/2010MWR3378.1.

Park, D.-S. R., J. Kim, K. Kang, and C. C. Nam, 2016: Highlighting socioeconomic damages caused by weakened tropical cyclones in the Republic of Korea. *Nat. Hazards*, **82**, 1301–1315, https://doi.org/10.1007/s11069-016-2244-x.

Pei, Y., and H. Jiang, 2018: Quantification of precipitation asymmetries of tropical cyclones using 16-yr TRMM observations. *J. Geophys. Res. Atmos.*, **123**, 8091–8114, https://doi.org/10.1029/2018JD028545.

Rappaport, E. N., 2014: Fatalities in the United States from Atlantic tropical cyclones: New data and interpretation. *Bull. Amer. Meteor. Soc.*, **95**, 341–346, https://doi.org/10.1175/BAMS-D-12-00074.1.

Schumacher, A., M. DeMaria, and J. Knaff, 2013: Summary of the new statistical-dynamical intensity forecast models

for the Indian Ocean and Southern Hemisphere and resulting performance. JTWC Project Final Rep. 1–11, http://rammb.cira.colostate.edu/research/tropical_cyclones/ships/docs/JTWC_project_final_report_oct_2013.docx.

Shimada, U., H. Owada, M. Yamaguchi, T. Iriguchi, M. Sawada, K. Aonashi, M. DeMaria, and K. D. Musgrave, 2018: Further improvements to the Statistical Hurricane Intensity Prediction Scheme using tropical cyclone rainfall and structural features. *Wea. Forecasting*, **33**, 1587–1603, https://doi.org/10.1175/WAF-D-18-0021.1.

Tuleya, R. E., M. DeMaria, and R. J. Kuligowski, 2007: Evaluation of GFDL and simple statistical model rainfall forecasts for U.S. landfalling tropical storms. *Wea. Forecasting*, **22**, 56–70, https://doi.org/10.1175/WAF972.1.

Willoughby, H. E., 2012: Distributions and trends of death and destruction from hurricanes in the United States, 1900–2008. *Nat. Hazards Rev.*, **13**, 57–64, https://doi.org/10.1061/(ASCE)NH.1527-6996.0000046.

Wingo, M. T., and D. J. Cecil, 2010: Effects of vertical wind shear on tropical cyclone precipitation. *Mon. Wea. Rev.*, **138**, 645–662, https://doi.org/10.1175/2009MWR2921.1.